

Evidence of production of keV Sn⁺ ions in the H₂ buffer gas surrounding an Sn-plasma EUV source

S Rai^{1,2} , K I Bijlsma^{1,2} , L Poirier^{2,3} , E de Wit¹ , L Assink^{1,2} , A Lassise²,
I Rabadán⁴ , L Méndez⁴ , J Sheil^{2,3} , O O Versolato^{2,3}  and R Hoekstra^{1,2,*} 

¹ Zernike Institute for Advanced Materials, University of Groningen, Nijenborgh 4, 9747 AG Groningen, The Netherlands

² Advanced Research Center for Nanolithography (ARCNL), Science Park 106, 1098 XG Amsterdam, The Netherlands

³ Department of Physics and Astronomy, and LaserLaB, Vrije Universiteit, De Boelelaan 1081, 1081 HV Amsterdam, The Netherlands

⁴ Laboratorio Asociado al CIEMAT de Física Atómica y Molecular en Plasmas de Fusión, Departamento de Química, Universidad Autónoma de Madrid, Cantoblanco E-28049 Madrid, Spain

E-mail: r.a.hoekstra@rug.nl

Received 7 November 2022, revised 13 February 2023

Accepted for publication 8 March 2023

Published 23 March 2023



Abstract

Charge-state-resolved kinetic energy spectra of Sn ions ejected from a laser-produced plasma (LPP) of Sn have been measured at different densities of the H₂ buffer gas surrounding a micro-droplet LPP. In the absence of H₂, energetic keV Sn ions with charge states ranging from 4+ to 8+ are measured. For the H₂ densities used in the experiments no appreciable stopping or energy loss of the ions is observed. However, electron capture by Sn ions from H₂ results in a rapid shift toward lower charge states. At the highest H₂ pressure of 6×10^{-4} mbar, only Sn²⁺ and Sn⁺ ions are measured. The occurrence of Sn⁺ ions is remarkable due to the endothermic nature of electron capture by Sn²⁺ ions from H₂. To explain the production of keV Sn⁺ ions, it is proposed that their generation is due to electron capture by metastable Sn^{2+*} ions. The gateway role of metastable Sn^{2+*} is underpinned by model simulations using atomic collision cross sections to track the charge states of Sn ions while traversing the H₂ buffer gas.

Keywords: ion-atom collisions, charge exchange, EUV source, laser-produced plasma

(Some figures may appear in colour only in the online journal)

1. Introduction

Sources of extreme ultraviolet (EUV) light are based on laser-produced plasma (LPP) of high temperatures (up to 50 eV) and

high free electron densities ($10^{19-21} \text{ cm}^{-3}$) in which highly charged ions are produced that are the atomic sources of the EUV radiation [1, 2]. For nanolithographic tools, the EUV wavelength of choice is 13.5 nm, which is dictated by the existence of high reflectivity multilayer optics [3, 4]. The element of choice for plasma generation of 13.5 nm radiation is Sn. Over a broad range of charge states (9+ to 15+), singly, doubly, and triply excited electronic configurations emit around 13.5 nm [5].

Subsequent to the desired production of EUV radiation, the plasma expands and generates energetic Sn ions [6], which if

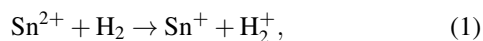
* Author to whom any correspondence should be addressed.



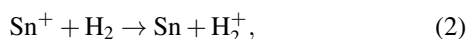
Original Content from this work may be used under the terms of the [Creative Commons Attribution 4.0 licence](https://creativecommons.org/licenses/by/4.0/). Any further distribution of this work must maintain attribution to the author(s) and the title of the work, journal citation and DOI.

impacting on the EUV collector optics may affect the lifetime of the optics. The energy and charge state distributions of Sn ions coming from the LPP contain information on the expansion dynamics of the plasma itself [7–11]. Moreover, accurate data on the energy distributions facilitate the determination of the fraction of the total energy that is carried by the plasma ions [12].

Typically, the energy spectrum of the emitted Sn ions peaks at a few keV with tails that may extend to tens of keV [11], except for Sn^+ and Sn^{2+} which are barely observed at higher energies above 0.5 keV. When an LPP is embedded in a stopping gas, only low-charged Sn ions are observed at much lower energies, which is a direct signature of charge exchange and collisional stopping, energy transfer from the Sn particles to the stopping gas. In this paper, we address the initial stage of the charge and energy redistribution in which charge exchange is active but the energy loss to the stopping gas is still negligible. This separation can be made if the cross sections for charge exchange are much larger than the ones for significant kinetic-energy transfer. For Sn^{q+} ions with $q \geq 3$ this assumption is not debated but in the case of $1+$ and $2+$ ions, the charge transfer cross sections for the reactions



and



are conventionally expected to be negligible because of the low scaled kinetic energies of the Sn ions ($\ll 100$ eV/u) and the considerable endothermicity of the reactions. The Franck Condon ionization potential of H_2 is 16.1 eV [13, 14], while the ionization potentials of Sn^+ and Sn are 14.6 and 7.3 eV [15], respectively. Thus, resonant electron capture by Sn^{2+} is endothermic by 1.5 eV and in the case of Sn^+ by no less than 8.7 eV.

Remarkable enough while indeed no appreciable signs of charge transfer by singly charged Sn ions (equation (2)) are found we will show an efficient production of Sn^+ ions out of the population of doubly charged Sn ions. Based on all available data the case is made that the Sn^+ ions are produced by electron capture by metastable Sn^{2+*} ions in the excited $[\text{Kr}]4d^{10}5s5p\ ^3\text{P}_J$ levels (the ground state of Sn^{2+} is $[\text{Kr}]4d^{10}5s^2\ ^1\text{S}_0$).

From an EUV source perspective, the actual abundances of singly and doubly charged Sn ions and thus, whether Sn^{2+} ions get converted by electron capture into Sn^+ , impacts the Sn ion mitigation because the penetration depth of the Sn ions into the H_2 buffer gas depends on the stopping cross sections. Recent stopping measurements [16] hint at appreciably larger stopping powers for Sn^+ than for Sn^{2+} ions.

This paper is organized as follows. First, the LPP source installed at ARCNL is briefly introduced with emphasis on the methods used to measure the charge-state dependent energy distributions of Sn^{q+} ions coming from the expanding LPP plasma. Thereafter the energy distributions as a function of

the H_2 buffer gas are presented with a focus on the Sn^+ ions, which present the evidence of the occurrence of charge exchange by Sn^{2+} ions. Finally based on potential-energy curves and Landau-Zener type calculations it is discussed that electron capture from H_2 by metastable $\text{Sn}^{2+*}(\ ^3\text{P}_J)$ ions is exothermic and likely to happen given the effective production of metastable $\text{Sn}^{2+*}(\ ^3\text{P})$ in collisions of Sn^{3+} on H_2 .

2. Experiment: methodology and data

The LPP EUV source used for the present set of experiments has been described in detail before [17]. The parts and features most relevant to this work are briefly recalled here. A tin reservoir, which is kept at a temperature of 260°C, is mounted on top of a vacuum chamber with a background vacuum of 10^{-7} mbar. In the H_2 buffer gas runs, molecular hydrogen pressures covering the range from 6×10^{-5} to 6×10^{-4} mbar have been used. At a repetition rate of 25 kHz droplets of pure, molten tin are pushed through a nozzle into the vacuum chamber. The stream of microdroplets with a diameter of 27 μm , first traverse a light sheet generated by a He-Ne laser. After frequency down-conversion to 10 Hz, the light scattered off the Sn droplets is used to trigger a 10-Hz Nd:YAG laser which creates the Sn plasma. The Nd:YAG laser system is operated at a wavelength of 1064 nm and produces pulses of approximately 10 ns full-width at half-maximum (FWHM). The spatial beam profile is Gaussian and is focused to a spot size of 100 μm FWHM onto the droplets in the center of the chamber. A laser pulse energy of 200 mJ yielding a power density of 3×10^{11} W cm^{-2} has been used in all experimental data presented in the following.

The energy distributions of the Sn^{q+} ions from the LPP are measured with a retarding field analyzer (RFA), more specifically a 4-grid Kimball Physics FC-73 RFA. The RFA is positioned at a distance of 68.5 cm from the LPP and at an angle of 64° with respect to the laser beam as illustrated in figure 1. The RFA is absolutely calibrated against an open, grid-less Faraday cup [18] to establish the integral transmission of the four grids. The same ‘bottom-up’ method as introduced by Poirier *et al* [19] is used to extract the kinetic-energy distributions for each individual charge state of tin ions from their joint overlapping energy distributions.

To interpret the ion energy spectra as a function of the H_2 pressure, one needs to know the relation between the pressure measured at the pressure gauge and the pressure (H_2 density) along the ions’ trajectory from the LPP to the ion detector. With the Monte-Carlo package MOLFLOW+ [20] developed at CERN we have calculated the H_2 density within the entire LPP vacuum chamber and all its additional vacuum tubing and equipment. The results of this simulation are shown in figure 2. Along the ion path, the average relative H_2 density is seen to be just 3% higher than the density at the position of the pressure gauge and to change by a few percent only over the full distance of 68.5 cm. Therefore, taking a constant density along the ions’ trajectory does not introduce significant

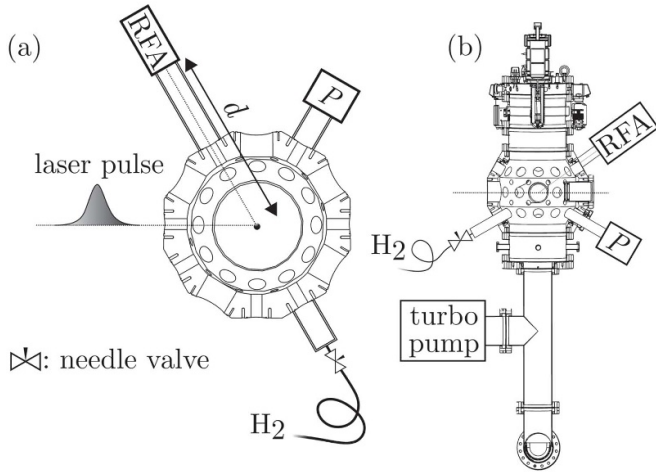


Figure 1. Schematic ((a): top view, (b): side view) of the LPP experiment to measure charge-state-specific ion spectra as a function of the pressure of the H_2 buffer gas embedding the LPP plasma. The distance d from plasma to the RFA type ion detector is 68.5 cm.

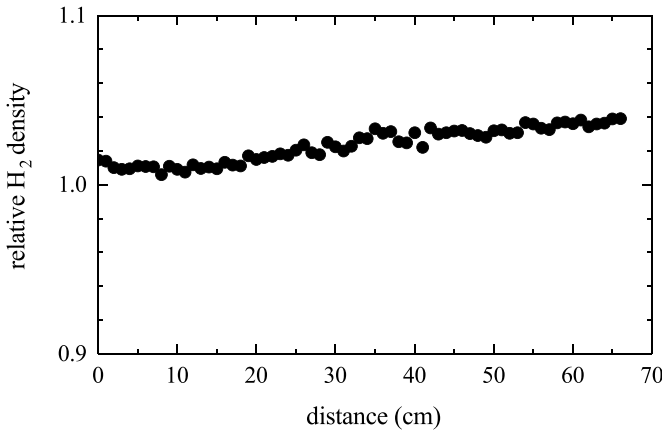


Figure 2. MOLFLOW+ Monte Carlo simulation results of the relative H_2 density, with respect to the density at the position of the pressure gauge, along the trajectory of Sn^{q+} ions flying from the LPP in the center of the vacuum chamber to the RFA detector, positioned at 68.5 cm from that center.

errors when calculating charge state distributions along those trajectories. The largest uncertainty will stem from the absolute H_2 density calibration of the pressure gauge, which is given by the manufacturer as 30%.

The energy distributions for all eight charge states are presented in figure 3 for five different H_2 pressures. Sn ions in charge states up to 8+ are observed in the RFA measurements. Note that the results labeled 10^{-6} mbar are the reference measurements with no H_2 gas surrounding the LPP plasma. The main points to be noted are that the spectra of Sn^{8+} , Sn^{7+} , and Sn^{6+} are rather narrow, peak at approximately 2 keV, and disappear with increasing H_2 pressure. In the absence of H_2 gas (grey spectra in figure 3) the spectra of Sn^{3+} , Sn^{2+} , and Sn^{+} are seen to extend to maximum kinetic energies of 1 keV for Sn^{3+} and ≈ 0.7 keV for Sn^{2+} and Sn^{+} . With increasing H_2 pressure a peak at 2 keV, similar to the 2-keV

peak characterizing the Sn^{8+} , Sn^{7+} , and Sn^{6+} spectra, grows into the Sn^{3+} , Sn^{2+} , and Sn^{+} spectra. Therefore the keV ions of Sn^{3+} , Sn^{2+} , and Sn^{+} observed in the energy spectra taken with a H_2 stopping gas around the LPP plasma must originate from Sn^{q+} ions with $q \geq 4$ by means of consecutive electron capture reactions. Last but not least, the emergence of energetic ($E \geq 1$ keV) Sn^{+} ions with increasing H_2 pressure is a clear sign that one-electron capture by Sn^{2+} (equation (1)) is not blocked by an anticipated endothermicity of the reaction and moreover even has a significant cross section.

3. Discussion

Before addressing the above points, one should realize that from an industrial source perspective, our experiments are performed at pressures representing the initial stages of the trajectories of Sn ions in the H_2 stopping gas after being ejected from the plasma. In this first phase, charge-exchange processes lower the average charge state of the ions rapidly before the ions have undergone appreciable energy loss. The validity of this approximation is implicit in the charge-state dependent energy spectra shown in figure 3 where the high energy peak is seen to remain at 2 keV whilst the charge state of the high energy ions decreases.

The reduction of average charge state without significant energy loss is illustrated in figure 4. This figure shows in its top panel the cumulative charge as a function of energy, while the bottom panel presents the number of particles as a function of energy. In the peak range (1–5 keV) the amount of charge measured at the RFA drops by approximately a factor of 4 when the H_2 pressure is raised to 6×10^{-4} mbar. In contrast to that the number of Sn ions having energies above 1 keV has not changed appreciably. The assumption that initially, charge transfer processes dominate over stopping and determine the changes in the charge-state dependent energy distributions therefore appears valid.

The pressure dependence of the particle-number distributions for all charge states from $q=8$ down to $q=1$ can be tracked by a set of eight differential equations of the type:

$$\frac{dN^{q+}}{dl} = n\sigma_{q+1 \rightarrow q}N^{(q+1)+} - n\sigma_{q \rightarrow q-1}N^{q+}, \quad (3)$$

with N^{q+} the number of Sn ions in charge state $q+$, n the H_2 target density, $\sigma_{q \rightarrow q-1}$ the cross section for charge exchange from charge state $q+$ to $(q-1)+$, and l the position along the ion's trajectory. With the exception of Sn^{3+} [21], no charge exchange data is available for Sn^{q+} ions colliding on H_2 . Therefore we decided to use the classical over-the-barrier model [22–24] to calculate estimates for $\sigma_{q \rightarrow q-1}$ cross sections for charge states $q \geq 4$ and which are found to be 62, 76, 88, 100, and 112 ($\times 10^{-16}$ cm²) for 4+, 5+, 6+, 7+, and 8+ Sn ions, respectively. Cross sections obtained with the over-the-barrier model present typically an upper-limit cross section as the model assumes that for impact parameters smaller than a specific distance capture happens with 100% probability. For endothermic charge-transfer reactions

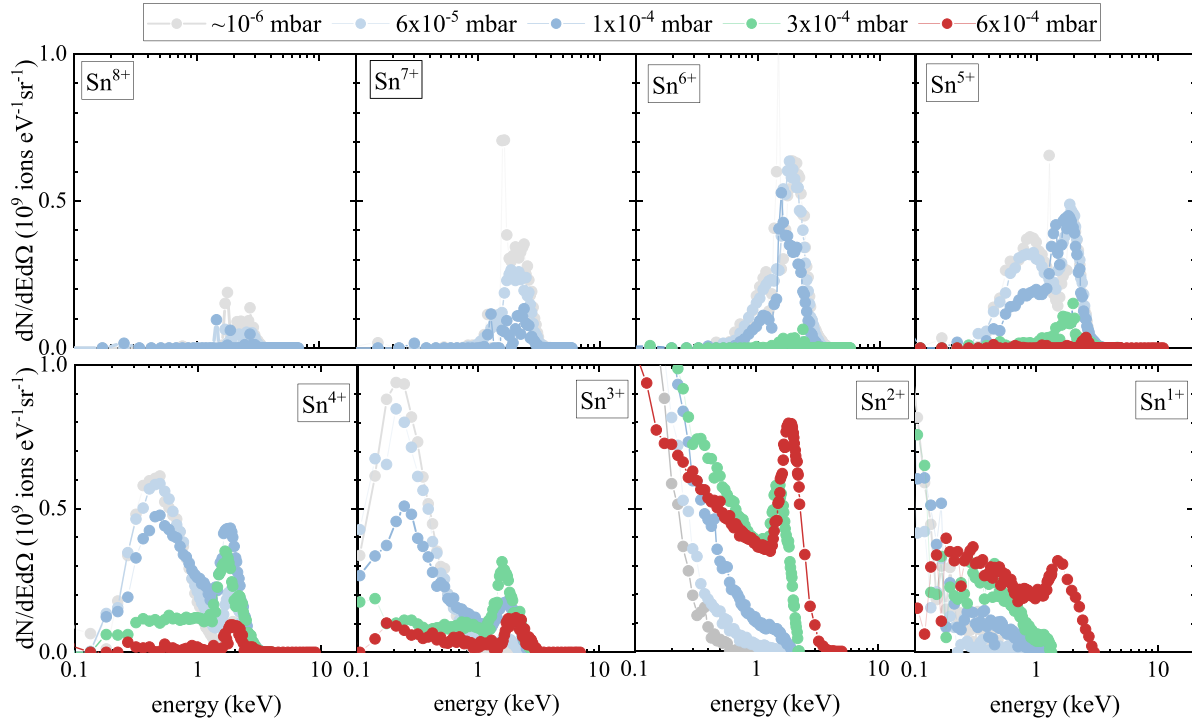


Figure 3. The yield of Sn^{q+} ions as a function of their kinetic energy in case of no H_2 gas and for H_2 buffer gas pressures in the range 6×10^{-5} to 6×10^{-4} mbar. The ions' flight path through the buffer gas is 68.5 cm.

cross sections are very small at low energies [25, 26], typically much smaller than 10^{-16} cm^2 . To illustrate the contribution of a non-zero cross section for Sn^{2+} ions a cross section of $0.1 \times 10^{-16} \text{ cm}^2$ has been used in the simulations. The results of a particle-number simulation are shown in figure 5. In line with the experimental data for energetic Sn ions ($E \geq 1 \text{ keV}$) (see figure 3) the charge-state fractions of energetic Sn ions swap from $q \geq 4$ to $q < 3$ over the pressure range of 10^{-4} to 10^{-3} mbar. In contrast to the experimental data, which show a considerable (20%) fraction of $1+$ ions at a pressure of 6×10^{-4} mbar, barely any Sn^{1+} ions are predicted. To obtain large Sn^{1+} populations matching the experimental data, a much larger cross section of order 10^{-15} cm^2 is required.

For an electron-capture reaction to have a large cross-section, the potential energy curves of the initial and final channels are required to cross one another at an internuclear distance between the ion and the target particle on the order of 10 a.u. A simplified picture, including only the Coulomb repulsion in the $\text{Sn}^+ - \text{H}_2^+$ exit channel, of the most relevant potential energy curves for $\text{Sn}^{2+} - \text{H}_2$ collisions is shown in figure 6.

In figure 6, the electronic potential energy of ground state $\text{Sn}^{2+}(5s^2 \ ^1\text{S})$ and H_2 is taken as reference for all other channels. As mentioned in the introduction the electron-capture channel $\text{Sn}^+(5s^2 5p \ ^2\text{P}) + \text{H}_2^+$ is endothermic by 1.5 eV at infinite internuclear distance between the particles. At shorter distances, due to the Coulomb repulsion between Sn^+ and H_2^+ the difference between both curves increases, and thus both potential energy curves do not cross underpinning the original

idea of resonant electron capture from H_2 by ground state $\text{Sn}^{2+}(5s^2 \ ^1\text{S})$ not being possible.

For metastable $\text{Sn}^{2+}(5s5p \ ^3\text{P})$ ions (Sn^{2+*}) the situation is very different. The $5s5p \ ^3\text{P}$ term lies about 7 eV (weighted average of the excitation energies of the $J = 0, 1$, and 2 levels of 6.64, 6.84, 7.34 eV, respectively [15]) above the ground state. Therefore at an internuclear distance R_c , there exists a curve crossing with the electron capture channel near 6 a.u., cf figure 6. Using this distance, one might estimate using the 'absorbing sphere' approximation [27, 28] a maximum cross section of $1.4 \times 10^{-15} \text{ cm}^2 (= 0.45 \pi R_c^2)$. This cross section is of similar order of magnitude as the one for $\text{Sn}^{3+} - \text{H}_2$ collisions [21], which indicates that one-electron capture by metastable Sn^{2+} ions is a potential gateway to produce singly charged Sn^+ ions.

Metastable Sn^{2+*} ions as a source for the production of Sn^+ ions by means of electron capture obviously requires large abundances of metastable Sn^{2+*} ions. In our earlier work on charge exchange in Sn^{3+} on H_2 [21], semiclassical calculations showed that electron capture populates directly, and at energies of a few keV almost solely ($\gg 95\%$), the metastable $\text{Sn}^{2+}(5s5p \ ^3\text{P})$ term. The latter point of the very high state selectivity of charge transfer in 1 to 10 keV Sn^{3+} on H_2 collisions was not explicitly discussed in that paper because then we focused on 10 to 100 keV collision energies. The predominant population of only one term is in line with existing data on other collision systems, all showing that at low energies well below 1 keV/u charge exchange becomes extremely state selective with a single state carrying almost all of the charge exchange cross section, e.g. [29–32]. As shown above, all keV

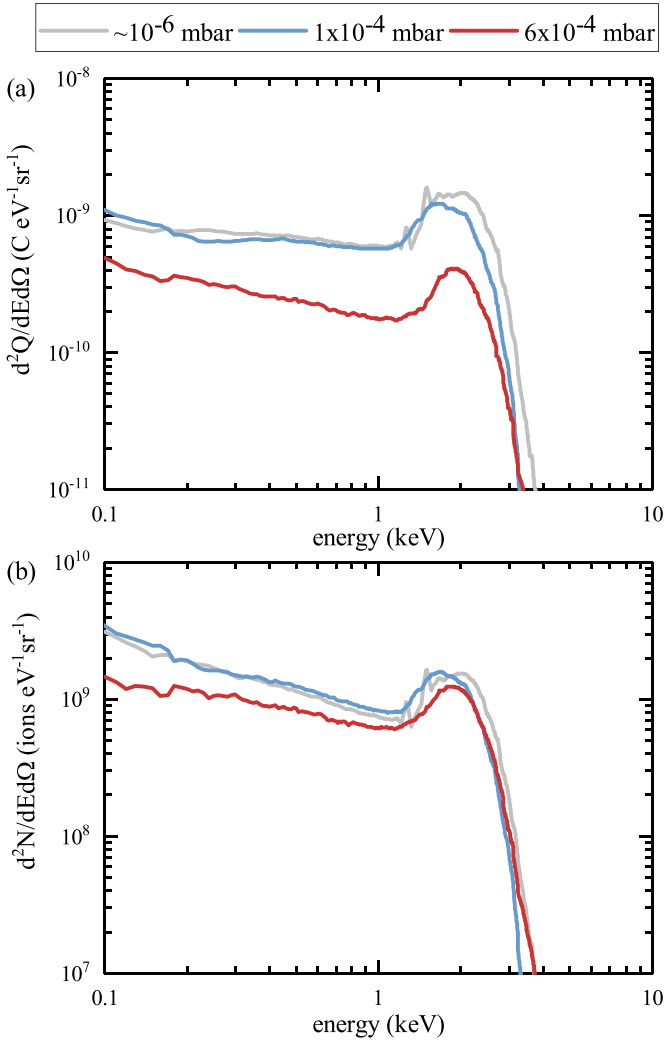


Figure 4. Top panel a: Total amount of charge as a function of Sn ion energy. Bottom panel b: Total number of ions as a function of Sn ion energy. Results are presented for no H_2 buffer gas present (labeled $\sim 10^{-6}$ mbar) and buffer gas pressures of 1×10^{-4} and 6×10^{-4} mbar. The path length through the buffer gas is 68.5 cm.

Sn ions of high charge state get rapidly converted to Sn^{3+} ions and which, by subsequent charge transfer, create metastable Sn^{2+*} ions. Metastable Sn^{2+*} are therefore abundantly produced in the stopping gas.

Transitions from the populated metastable $5s5p^3P_{0,1,2}$ levels to the ground state $5s^2^1S$ are spin forbidden. However, how long are their lifetimes with respect to the time between subsequent collisions? For $J = 0$ and $J = 2$, the transitions are also symmetry forbidden and thus the levels are expected to be very long-lived. While $J = 0$ to $J' = 0$ are truly forbidden, $J = 2$ to $J' = 0$ transitions still exhibit small transition probabilities [33]. To get an order of magnitude estimate of the lifetime of the $Sn^{2+}5s5p^3P_2$ level, we performed a basic FAC (Flexible Atomic Code [34]) calculation. The calculation predicts a lifetime of the order of 10–100 s. This lifetime is very long compared to typical flight times in the experiment which are in the range of a few to a few tens of μs . For a heavy species such as Sn where the spin–orbit coupling is very significant,

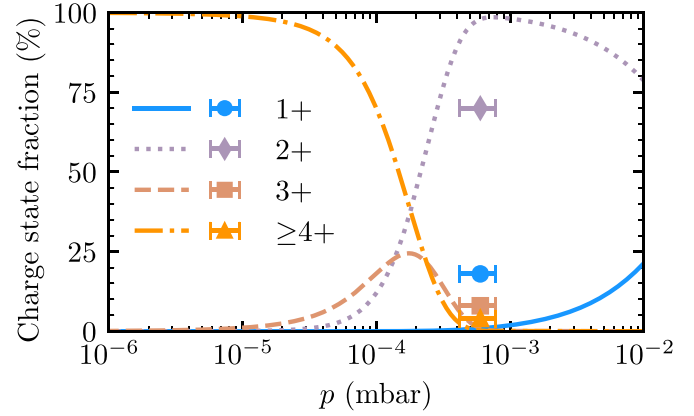


Figure 5. Simulated charge state fractions of energetic Sn^{q+} ions detected at a distance of 68.5 cm from the LPP plasma as a function of H_2 buffer pressure. For $q \geq 4$ the actual q specific fractions as measured at $p = 10^{-6}$ mbar (see figure 3) were used as input in solving the set of differential equations (equation (3)). Solid points show the experimental LPP data.

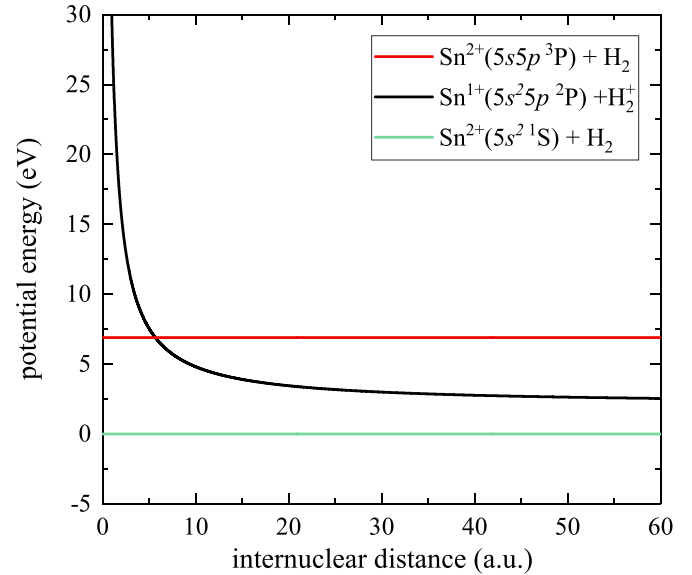


Figure 6. Schematic potential energy curves of relevant electronic channels in $Sn^{2+} + H_2$ collisions as a function of the internuclear distance between the Sn^{2+} ion and the H_2 molecule which is considered to be a point-like particle.

the $J = 1$ level is expected to have by far the shortest lifetime of the three levels of the 3P term as it can decay via a $\Delta J = 1$ transition to the ground state. For the 3P_1 theoretical lifetimes are reported of approximately 100 [35], 150 [36] and 200 ns [37]. In a beam foil experiment, [38] the decay was not observed indicating that the lifetime is much longer than 45 ns, consistent with the theoretical values.

During a period of one lifetime of 150 ns (average of the reported values), a 2 keV Sn particle travels a distance of approximately 0.8 cm. For a first estimation of the role of $J = 1$ metastables, we take three times the lifetime, a period after which 95% of the $J = 1$ metastables has decayed to the ground state. The associated flight path of the 2 keV Sn particle is

2 cm. This path length should be compared to the mean free path (λ_F) of the particles which is equal to $(n\sigma_{21})^{-1}$. For the highest pressure used here of 6×10^{-4} mbar (1.5×10^{13} H₂ molecules per cm³) and a σ_{21} of 10×10^{-16} cm² (discussed in the next paragraphs) one finds $\lambda_F \approx 67$ cm. Therefore only a very small fraction of the originally $J = 1$ metastables will undergo a collision with a H₂ molecule before having decayed to the ground state. Thus, in the experiments presented here the $J = 1$ metastables do not play an important role. Industrial sources operate at orders of magnitude higher H₂ pressures. For illustration, a pressure of say 1 mbar corresponds to a mean free path λ_F of ≈ 0.04 cm and therefore the opposite situation occurs where barely any of the $J = 1$ metastables have decayed.

For each of the three J levels we performed a basic 2-state Landau-Zener model calculation [29] to obtain J -dependent cross sections for electron capture by metastable Sn^{2+*} ions. For the coupling matrix element the generic form of the expression derived for atomic hydrogen targets [27] was used. The correction for the different ionization potentials I_H and I_{H_2} of H and H₂, respectively, is done as in references [27, 28] by scaling the coupling matrix element by $(I_{H_2}/I_H)^2$. The H₂ molecules are assumed all to be in the ground $\nu = 0$ vibrational level, because for H₂ molecules the vibrational level spacing is much larger (about 0.5 eV between $\nu = 0$ and $\nu = 1$) than the thermal energy (0.03 eV) of H₂ gas at room temperature. However instead of the prefactor of 9.41 we used a prefactor of 5.48 as proposed by Kimura *et al* [28] after optimization of Landau-Zener model calculations to their low-energy electron capture experiments on He. Other, early estimations more geared to lower charge state ions predicted even smaller prefactors [39, 40]. Therefore, we decided to use 5.48 as this value is in between those and it is experimentally benchmarked for another two-electron target. A different prefactor does not change the maximum cross section but shifts the position of the maximum cross section toward higher (larger prefactor) or lower (smaller prefactor) collision energy. The J -dependent cross section results are summarized in figure 7.

To solve the set of differential equations, equation (3), the Sn^{2+*} population needs to be divided over its three J level populations. The J dependent populations are available from the theoretical studies in our earlier work [21]. As that data was not explicitly shown in our earlier work, it is presented here in figure 8. From the figure it is seen that the population is not statistical, only at the lowest collision energies the distribution tends toward a statistical one. For the simulations, an average energy of the Sn³⁺ ions of 2 keV is used, for which according to figure 8 the population fractions of $J = 0, 1$, and 2 are 45%, 20% and 35%.

In addition, for the $J = 1$ level it is assumed that it decays to the ground state before a next charge-changing collision occurs, thus with this $J = 1$ level we associate the Sn²⁺ ground state capture cross section. For $J = 0$ and 2 the calculated cross sections depicted in figure 7 are used. Figure 9 shows the results of the simulations which now explicitly include metastable Sn^{2+*} ions. As can be seen from the figure, a rapid increase of the fraction of Sn⁺ is predicted. Now with the inclusion of Sn^{2+*} metastables the charge state fractions at

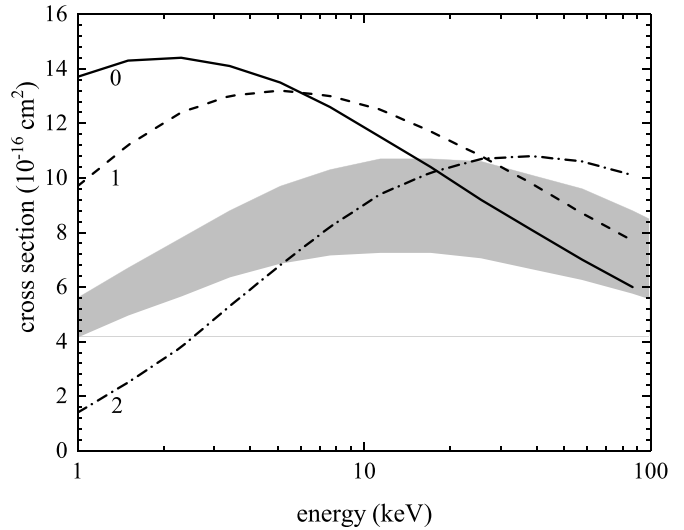


Figure 7. Cross sections for one-electron capture in 1 to 100 keV Sn²⁺ ($5s5p^3P_J$) collisions with H₂ according to our Landau-Zener model calculations. The solid, dashed, and dashed-dotted lines correspond to the J levels, with J is 0, 1, and 2, respectively. The grey band represents $(2J+1)$ weighted average cross sections, with the upper limits of the band assuming the $J = 1$ level fully contributing, and the lower limits of the band are defined by assuming no contribution by $J = 1$.

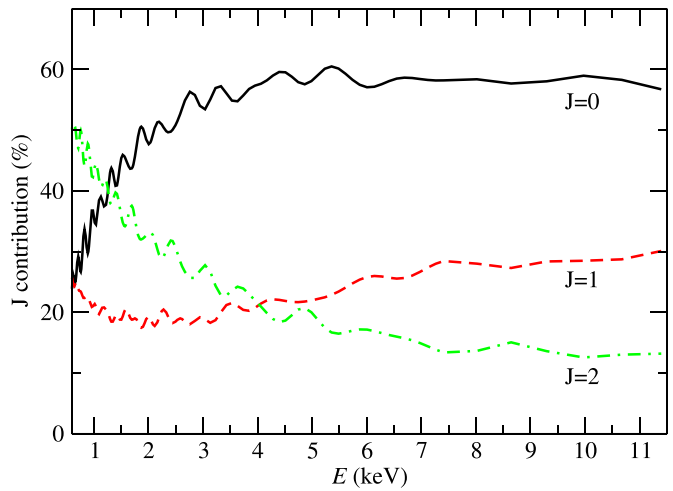


Figure 8. Calculated [21] J -dependent population fractions of the metastable Sn^{2+*} ($5s5p^3P_J$) levels produced by one-electron capture in Sn³⁺ collisions on H₂.

6×10^{-4} mbar are in line with the experimental data. The simulations appear to indicate that the singly charged Sn ions get produced at pressures somewhat lower than seen in the experiment. However, this is likely a result of the fact that we have used upper limits for the electron capture cross sections for Sn ions in charge states of $q \geq 4$. Smaller cross sections will shift the curves in figure 9 to the right to higher pressures for as equation (3) indicates it is the product of target density and cross section that factors into the differential equations. For an optimal comparison between experiment and simulation, charge exchange cross sections for Sn^{q+} ions in

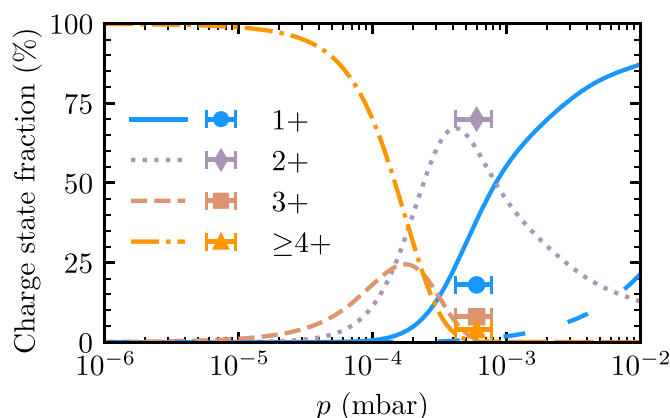


Figure 9. Simulated charge state distributions of energetic Sn^{q+} ions detected at a distance of 68.5 cm from the LPP plasma as a function of H_2 buffer pressures, assuming that all Sn^{2+} ions are produced in the metastable $5s5p\ ^3\text{P}$ term with a distribution over its J levels as shown in figure 8. For $q \geq 4$ the actual q specific fractions as measured at $p = 10^{-6}$ mbar (see figure 3) were used as input in solving the set of differential equations. For ease of comparison, the dashed blue line shows the Sn^{1+} ion fraction if no metastables are included (taken from figure 5). Solid points show the experimental LPP data.

charge states of $q \geq 4$ are called for. Nevertheless, the present simulations clearly highlight the key role of metastable Sn^{2+*} ions in the production of energetic keV Sn^{1+} ions by means of consecutive charge exchange starting from energetic highly charged Sn^{q+} ions with charge states of $q \geq 4$ ejected from the LPP into the surrounding H_2 buffer gas.

4. Conclusion

We have investigated the evolution of charge-state-resolved kinetic energy spectra of Sn ions ejected from a LPP of Sn as a function of the density of the H_2 buffer gas surrounding the plasma. Without H_2 being present, energetic 1 to 5 keV Sn ions in charge states of 4+ to 8+ are detected. Sn ions in lower charge states are absent at energies above 1 keV. However, at the highest H_2 pressure of 6×10^{-4} mbar, no highly charged Sn ions are measured anymore at energies above 1 keV, only Sn^{2+} and Sn^{1+} ions are observed. The low-charged energetic Sn ions are produced by a series of consecutive electron capture processes. Therefore, in particular, the presence of Sn^{1+} ions is remarkable because electron capture by Sn^{2+} ions from H_2 is endothermic and thus very unlikely to happen at keV energies, which from an atomic collision perspective are very low-energies. To explain the production of keV Sn^{1+} ions, electron capture by metastable Sn^{2+*} ions is inferred. Previous work on Sn^{3+} — H_2 collisions [21] indicates that one-electron capture by Sn^{3+} ions populates primarily Sn^{2+} ions in metastable states. Using 2-state Landau Zener model cross sections for capture by the metastables, the key role of metastable Sn^{2+} is highlighted by model simulations using atomic collision cross sections to track the charge states of Sn ions while traversing the H_2 buffer gas.

The production of Sn^{1+} ions in the buffer gas is of relevance from an industrial EUV source perspective. It shifts the charge state balance away from Sn^{2+} toward Sn^{1+} . As Sn^{1+} ions have a larger stopping cross section than Sn^{2+} ions [16], the production of Sn^{1+} ions is beneficial to stopping Sn ions escaping from an LPP plasma in a high charge state.

Data availability statement

The data cannot be made publicly available upon publication because they are not available in a format that is sufficiently accessible or reusable by other researchers. The data that support the findings of this study are available upon reasonable request from the authors.

Acknowledgments

This work is part of the research portfolio of the Advanced Research Center for Nanolithography (ARCNL), a public-private partnership between the University of Amsterdam (UvA), the Vrije Universiteit Amsterdam (VU), the University of Groningen (RuG), the Netherlands Organization for Scientific Research (NWO), and the semiconductor equipment manufacturer ASML. The project is co-financed by Holland High Tech with PPS allowance for research and development in the top sector HTSM. The theoretical work of I R and L M was partially supported by Ministerio de Economía and Competitividad (Spain), Project No. FIS2017-84684-R. The computational support by the Centro de Computación Científica of UAM is also acknowledged.

ORCID iDs

S Rai <https://orcid.org/0000-0003-0391-8485>
 K I Bijlsma <https://orcid.org/0000-0002-9440-4035>
 L Poirier <https://orcid.org/0000-0001-7177-8926>
 E de Wit <https://orcid.org/0000-0001-7638-2824>
 L Assink <https://orcid.org/0000-0003-1165-5996>
 I Rabadán <https://orcid.org/0000-0001-6737-4742>
 L Méndez <https://orcid.org/0000-0003-1391-2634>
 J Sheil <https://orcid.org/0000-0003-3393-9658>
 O O Versolato <https://orcid.org/0000-0003-3852-5227>
 R Hoekstra <https://orcid.org/0000-0001-8632-3334>

References

- [1] O'Sullivan G et al 2015 *J. Phys. B: At. Mol. Opt. Phys.* **48** 144025
- [2] Versolato O O 2019 *Plasma Sources Sci. Technol.* **28** 083001
- [3] Bajt S, Alameda J B, Barbee Jr T W, Clift W M, Folta J A, Kaufmann B and Spiller E A 2002 *Opt. Eng.* **41** 1797
- [4] Huang Q, Medvedev V, van de Kruijs R, Yakshin A, Louis E and Bijkerk F 2017 *Appl. Phys. Rev.* **4** 011104
- [5] Torretti F et al 2020 *Nat. Commun.* **11** 2334
- [6] Hemminga D J, Poirier L, Basko M M, Hoekstra R, Ubachs W, Versolato O O and Sheil J 2021 *Plasma Sources Sci. Technol.* **30** 105006
- [7] Fujioka S et al 2005 *Appl. Phys. Lett.* **87** 241503

- [8] Murakami M, Kang Y, Nishihara K, Fujioka S and Nishimura H 2005 *Phys. Plasmas* **12** 062706
- [9] Giovannini A Z, Gambino N, Rollinger B and Abhari R S 2015 *J. Appl. Phys.* **117** 033302
- [10] Deuzeman M J et al 2017 *J. Appl. Phys.* **121** 103301
- [11] Bayerle A et al 2018 *Plasma Sources Sci. Technol.* **27** 045001
- [12] Bakshi V (ed) 2018 *EUV Lithography* 2nd edn (Bellingham, WA: SPIE Press)
- [13] Sharp T E 1971 *At. Data Nucl. Data Tables* **2** 119–69
- [14] Wacks M 1964 *J. Res. Natl Bur. Stand. A* **68** 631
- [15] Kramida A, Ralchenko Y and Reader J (NIST ASD Team) 2015 *NIST Atomic Spectra Database (ver. 5.3)* (Gaithersburg, MD: National Institute of Standards and Technology) (available at: <http://physics.nist.gov/asd>) (Accessed 21 October 2022)
- [16] Abramenko D, Spiridonov M, Krainov P, Krivtsun V, Astakhov D, Medvedev V, van Kampen M, Smeets D and Koshelev K 2018 *Appl. Phys. Lett.* **112** 164102
- [17] Kurilovich D, Klein A L, Torretti F, Lassise A, Hoekstra R, Ubachs W, Gelderblom H and Versolato O O 2016 *Phys. Rev. Appl.* **6** 014018
- [18] Poirier L, Bayerle A, Lassise A, Torretti F, Schupp R, Behnke L, Mostafa Y, Ubachs W, Versolato O O and Hoekstra R 2022 *Appl. Phys. B* **128** 39
- [19] Poirier L, Lassise A, Mostafa Y, Behnke L, Braaksma N, Assink L, Hoekstra R and Versolato O O 2022 *Appl. Phys. B* **128** 135
- [20] Kersevan R and Ady M 2019 Recent developments of Monte-Carlo codes MolFlow+ and SynRad+ *10th Int. Particle Accelerator Conf. (IPAC'19) (Melbourne, Australia)* (<https://doi.org/10.18429/JACoW-IPAC2019-TUPMP037>)
- [21] Rai S, Bijlsma K I, Rabadán I, Méndez L, Wolff P A J, Salverda M, Versolato O O and Hoekstra R 2022 *Phys. Rev. A* **106** 012804
- [22] Mann R, Folkmann F and Beyer H F 1981 *J. Phys. B: At. Mol. Phys.* **14** 1161
- [23] Ryufuku H, Sasaki K and Watanabe T 1980 *Phys. Rev. A* **21** 745
- [24] Niehaus A 1986 *J. Phys. B: At. Mol. Phys.* **19** 2925–37
- [25] Imai M, Iriki Y and Itoh A 2013 *Fusion. Sci. Technol.* **63** 392
- [26] Lomsadze R, Gochitashvili M and Kezerashvili R 2015 *Phys. Rev. A* **92** 062703
- [27] Olson R E and Salop A 1976 *Phys. Rev. A* **14** 579
- [28] Kimura M, Iwai T, Kaneko Y, Kobayashi N, Matsumoto A, Ohtani S, Okuno K, Takagi S, Tawara H and Tsurubuchi S 1984 *J. Phys. Soc. Japan* **53** 2224
- [29] Janev R K and Winter H 1985 *Phys. Rep.* **117** 265
- [30] Fritsch W and Lin C 1991 *Phys. Rep.* **202** 1–97
- [31] Stancil P C, Turner A R, Cooper D L, Schultz D R, Rakovic M J, Fritsch W and Zygelman B 2001 *J. Phys. B: At. Mol. Opt. Phys.* **34** 2481
- [32] Hoekstra R, Anderson H, Blik F W, von Hellermann M, Maggi C F, Olson R E and Summers H P 1998 *Plasma Phys. Control. Fusion* **40** 1541
- [33] Sobelman I I 1979 *Atomic Spectra and Radiative Transitions* (Berlin: Springer)
- [34] Gu M F 2008 *Can. J. Phys.* **86** 675
- [35] Haris K and Tauheed A 2012 *Phys. Scr.* **85** 055301
- [36] Curtis L J, Matulioniene R, Ellis G and Froese Fischer C 2000 *Phys. Rev. A* **62** 052513
- [37] Colón C and Alonso-Medina A 2010 *J. Phys. B: At. Mol. Opt. Phys.* **43** 165001
- [38] Kernahan J A, Pinnington E H, Ansbacher W and Bahr J L 1985 *Nucl. Instr. Meth. Phys. Res. B* **9** 616
- [39] Olson R E, Smith F T and Bauer E 1971 *Appl. Opt.* **10** 1848–55
- [40] Butler S E and Dalgarno A 1980 *Astrophys. J.* **241** 838–43